

# Decoherence and energy flow in the sunburst quantum Ising model

Alessio Franchi, Davide Rossini, and Ettore Vicari

Dipartimento di Fisica dell'Università di Pisa and INFN, Largo Pontecorvo 3, I-56127 Pisa, Italy

Authors are listed in alphabetic order

**Abstract.** We study the post-quench unitary dynamics of a quantum sunburst spin model, composed of a transverse-field quantum Ising ring which is suddenly coupled to a set of independent external qubits along the longitudinal direction, in a way to respect a residual translation invariance and the Ising  $\mathbb{Z}_2$  symmetry. Starting from the different equilibrium quantum phases of the system, we characterize the decoherence and the energy storage in the external qubits, which may be interpreted as a probing apparatus for the inner Ising ring. Our results show that, in proximity of the quantum transitions of the Ising ring, either first-order or continuous, it is possible to put forward dynamic FSS frameworks which unveil peculiar scaling regimes, depending on the way in which the large-size limit is taken: either by fixing the number  $n$  of probing qubits, or their interspace distance  $b$ . In any case, the dependence of the various observables on  $n$  can be reabsorbed into a redefinition of the quench parameter by a  $\sqrt{n}$  prefactor. We also address the role of a nearest-neighbor coupling between the external qubits.

## 1. Introduction

The recent progress achieved by quantum simulators in carefully controlling the dynamics of an increasing number of qubits has enticed further theoretical studies on the coherent time evolution of quantum correlations and energy exchanges of finite-size quantum systems (see, e.g., Refs. [1, 2, 3, 4, 5]). On the one hand, a deeper understanding of the decoherence dynamics and spreading of entanglement correlations is of fundamental importance, both for quantum-information purposes and for the improvement of energy conversion in complex networks [5, 6]. On the other hand, the study of the energy storage among distinguished parts of a quantum system, exploring different geometric schemes, is relevant for quantum-thermodynamical purposes [7, 8], as well as for the efficiency optimization of recently developed quantum batteries [9]. In experiments with ultracold atoms, such quantities can be also used to monitor the time evolution of a finite amount of interacting qubits [10, 11].

However, in any experimental setup, one is interested in bringing to light the properties of the system under study, carefully minimizing the perturbations ascribed to the devices employed to probe it. As the superposition principle drives disjoint parts of the same network to be entangled during the time evolution, a collective framework in which the system and the probing apparatus are treated on the same footing is often necessary to correctly describe the evolution of the overall setup [12]. In this regime, it is interesting to find out how much information we may retrieve by considering the coherent collective dynamics of the system and the probing apparatus as a whole, but only looking at the quantum devices used to probe the system under analysis. Among the various schemes of composite systems that can be useful to address this kind of issues, we mention the so-called *central spin* models, which have attracted a great deal of attention in the recent years, both theoretically and experimentally (see, e.g., Refs. [13, 14, 15, 16, 17, 18, 19, 20, 21, 22, 23, 24, 25, 26, 27, 28, 29, 30, 31, 32, 1]).

In this work we focus on an alternative lattice configuration, in the class of the *sunburst* quantum models (for a sketch see Fig. 1), in which many independent spins are longitudinally coupled to a quantum Ising ring. Specifically, we consider a set of  $L$  spin-1/2 quantum objects (qubits) disposed in a ring geometry (blue dots), interacting through nearest-neighbor Ising-like interactions. We probe the system by means of  $n$  equally-spaced qubits (being  $b$  their interspace distance), completely independent of each other, to which we will refer in the following as the *ancillary* spins or simply the *external* spins (red dots). A thorough analysis of the equilibrium ground-state properties of this apparatus has been recently performed in Ref. [33]. Here we are interested in investigating the out-of-equilibrium dynamics triggered by a sudden quench of an external parameter  $\kappa$ , which couples the system under study with the monitoring devices. When the monitoring devices act as a small perturbation, leading to *soft* quenches, the out-of-equilibrium quantum evolution is studied within dynamic finite-size scaling frameworks, which turn out to be particularly effective to infer dynamic scaling laws for finite-size systems [34, 1]. In particular, two different dynamic FSS

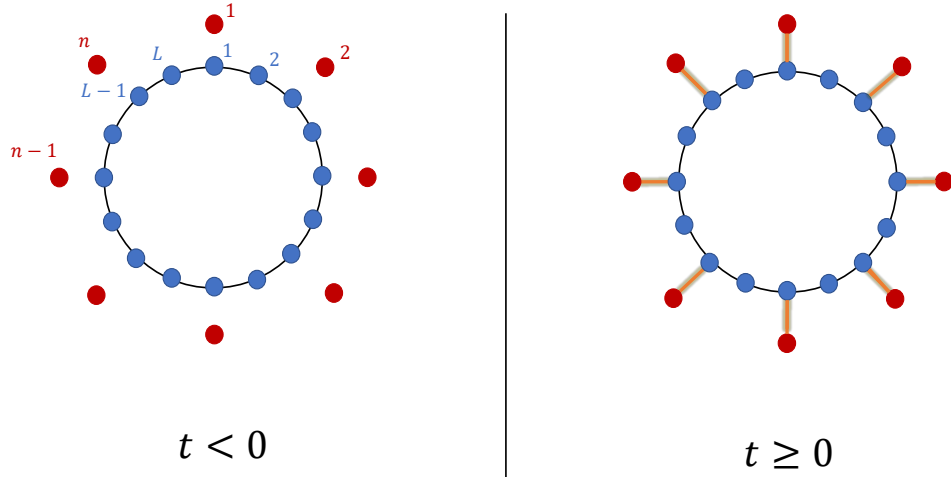


**Figure 1.** Sketch of the setup studied in this paper. For times  $t < 0$  (left side), the system is initialized and left in the ground-state configuration where ancillary spins ( $\mathcal{A}$ , red dots) belonging to the probing apparatus are initially decoupled from the Ising ring qubits ( $\mathcal{I}$ , blue dots). At time  $t = 0$ , the ring and the external spins are suddenly coupled together (thick red lines) by quenching the Hamiltonian parameter  $\kappa$  governing the  $\mathcal{I}$ - $\mathcal{A}$  interaction, thus unitarily driving the global system out of equilibrium (right side). In the figure, we set  $L = 16$ ,  $n = 8$ , and  $b = 2$ , see text.

limits can be defined at large sizes, either by keeping the number  $n$  of external qubits fixed or by maintaining their interspace distance  $b$  constant. We have carried out a careful FSS study of both limits, when the ring system is close to either continuous or first-order quantum transitions (CQTs or FOQTs, respectively) of the Ising ring. Moreover, we have considered quenches in the Ising-disordered phase. In any case, the dependence of observables on  $n$  can be always taken into account by a proper rescaling of the parameter  $\kappa$  by a  $\sqrt{n}$  prefactor. We also discuss the many-body dynamics arising from *hard* quenches, when the ancillary system introduces a relatively large amount of energy with respect to the energy differences of the lowest levels of the Ising ring. Finally, we address the role of a nearest-neighbor coupling between the external qubits.

The paper is organized as follows. In Sec. 2 we describe the setup of the model under analysis: the lattice Hamiltonian, the quench protocol, and the observables addressed during time evolution. In the next two sections we put forward a dynamic FSS framework that holds for systems close to a CQT (Sec. 3) and to a FOQT (Sec. 4), and support our theory with numerical results based on exact diagonalization. In Sec. 5 we show some results at fixed  $b$  in the disordered phase. In the last part of this work, we focus on hard quenches, comparing our results with the ones obtained when consecutive monitoring qubits also interact among themselves (Sec. 6). Finally, our conclusions are drawn in Sec. 7.

## 2. System setup

### 2.1. The lattice Hamiltonian

We are going to address some properties of the unitary out-of-equilibrium quantum dynamics of an Ising ring coupled to a set of external qubits along the longitudinal axis, which is ruled by the following global lattice Hamiltonian:

$$\hat{H} = \hat{H}_{\mathcal{I}} + \hat{H}_{\mathcal{A}} + \hat{H}_{\mathcal{IA}}. \quad (1)$$

The first term  $\hat{H}_{\mathcal{I}}$  describes a standard ferromagnetic Ising ring ( $\mathcal{I}$ ) in a transverse field, with  $L$  sites,

$$\hat{H}_{\mathcal{I}} = -J \sum_{i=1}^L \hat{\sigma}_i^{(1)} \hat{\sigma}_{i+1}^{(1)} - g \sum_{i=1}^L \hat{\sigma}_i^{(3)}, \quad (2)$$

where  $\hat{\sigma}_i^{(k)}$  (with  $k = 1, 2, 3$ ) denote the spin-1/2 Pauli matrices on the  $i$ th the lattice site, while  $\hat{\sigma}_{L+1}^{(k)} = \hat{\sigma}_1^{(k)}$ , since we are considering periodic boundary conditions (PBC). In the following we set  $\hbar = 1$ ,  $J = 1$  as the energy scale,  $a = 1$  as the lattice spacing, and take  $g > 0$  without loss of generality.

The Ising model is a paradigmatic quantum lattice system where fundamental issues related to the physics of quantum many-body networks can be thoroughly investigated, given our extended knowledge of its quantum phases and correlations, both in the thermodynamic and FSS limit [35, 1]. The ground state exhibits a zero-temperature CQT at  $g = g_{\mathcal{I}}$  belonging to the  $(d+1)$ -dimensional Ising universality class, separating a ferromagnetic phase ( $g < g_{\mathcal{I}}$ ) from a disordered phase ( $g > g_{\mathcal{I}}$ ). In the one-dimensional case, the quantum phase transition is located at  $g_{\mathcal{I}} = 1$ . Close to the quantum critical point (QCP), the system develops long-range correlations  $\xi$ , diverging as  $\xi \sim |g - g_{\mathcal{I}}|^{-\nu}$ , where  $\nu = y_g^{-1} = 1$  and  $y_g$  is the renormalization group (RG) exponent associated with the difference  $g - g_{\mathcal{I}}$ . The gap between the ground-state energy and the first excited state  $\Delta_{\mathcal{I}}$  is instead suppressed as  $\Delta_{\mathcal{I}} \sim \xi^{-z}$  close to the CQT (here  $z$  denotes the dynamic critical exponent,  $z = 1$ ). Consequently, for finite-size systems the gap is power-law suppressed as  $\Delta_{\mathcal{I}}(g = g_{\mathcal{I}}, L) = \pi/(2L) + O(L^{-2})$  at the QCP, whereas it vanishes exponentially at a FOQT when the boundary conditions do not favor any of the phases  $\Delta_{\mathcal{I}}(g < g_{\mathcal{I}}, L) \approx e^{-c(g)L}$ , as in the case of PBC [36, 37].

The second term  $\hat{H}_{\mathcal{A}}$  in Eq. (1) characterizes the energy of  $n$  independent ancillary ( $\mathcal{A}$ ) spin-1/2 systems (qubits), acting as quantum monitoring devices for the ring system under analysis,

$$\hat{H}_{\mathcal{A}} = -\frac{\delta}{2} \sum_{i=1}^n \hat{\Sigma}_i^{(3)}, \quad (3)$$

where  $\hat{\Sigma}_i^{(k)}$ s (with  $k = 1, 2, 3$ ) still represent Pauli matrices on the  $i$ th monitoring spin. The coupling  $\delta$  parameterizes the energy variation defined by the flip of a single qubit, which is the elementary excitation within the ensemble of the  $n$  independent qubits.

The last term  $\hat{H}_{\mathcal{IA}}$  couples together the ring system with the ancillary qubits along the longitudinal direction. In our analysis, the number  $n$  of equally-spaced spins is

always commensurate with the length  $L$  of the Ising ring, so that each pair of consecutive qubits is separated by a fixed distance  $b = L/n$ . It reads as follows

$$\hat{H}_{\mathcal{I}A} = -\kappa \sum_{i=1}^n \hat{\sigma}_{x=ib}^{(1)} \hat{\Sigma}_i^{(1)}, \quad (4)$$

where  $\kappa$  parameterizes the intensity of the coupling.

The model is characterized by a  $\mathbb{Z}_2$  symmetry under a global spin flip of both the ring and the ancillary spins, identified by the parity operator

$$\hat{P} = \left( \bigotimes_{i=1}^L \hat{\sigma}_i^{(3)} \right) \left( \bigotimes_{j=1}^n \hat{\Sigma}_j^{(3)} \right), \quad (5)$$

which acts on the Pauli operators as

$$\hat{P} \hat{\sigma}_i^{(1)} \rightarrow -\hat{\sigma}_i^{(1)}, \quad \hat{P} \hat{\Sigma}_i^{(1)} \rightarrow -\hat{\Sigma}_i^{(1)}, \quad (6a)$$

$$\hat{P} \hat{\sigma}_i^{(2)} \rightarrow -\hat{\sigma}_i^{(2)}, \quad \hat{P} \hat{\Sigma}_i^{(2)} \rightarrow -\hat{\Sigma}_i^{(2)}, \quad (6b)$$

$$\hat{P} \hat{\sigma}_i^{(3)} \rightarrow \hat{\sigma}_i^{(3)}, \quad \hat{P} \hat{\Sigma}_i^{(3)} \rightarrow \hat{\Sigma}_i^{(3)}. \quad (6c)$$

We point out that the global Hamiltonian (1) is left invariant under a change in the sign of  $\delta$  and/or  $\kappa$ , after a proper redefinition of the Pauli matrices. Thus, without loss of generality, in our analysis we will restrict ourselves to the cases  $\delta, \kappa \geq 0$ .

As mentioned in the introduction, the overall setup realizes the same lattice configuration as the sunburst quantum Ising model, whose equilibrium ground-state properties have been addressed in Ref. [33]. In a time-dependent perspective, the equilibrium limit corresponds to an adiabatically slow dynamics for finite-size systems. In contrast, here we are going to focus on the out-of-equilibrium decoherence properties and energy exchanges from the point of view of the ancillary spins, aiming at perceiving the capability of these probes to retrieve information on the Ising ring system under study, and in particular its equilibrium quantum phases before the quench. To this purpose, we consider two different dynamic FSS limits, depending on the parameters we decide to maintain fixed with increasing the lattice size  $L$  of the ring [33]:

- (i) We keep the number  $n = L/b$  of ancillary spins fixed while increasing  $L$ , thus the spins probing the ring get diluted in the FSS limit. The bulk properties of the Ising ring system (such as the location of the QCP or the equilibrium phase diagram) are left unchanged by the presence of the probing devices.
- (ii) We keep  $b$  fixed, so that the number of external qubits increases linearly with the ring size  $L$ . In this case, the qubits are expected to modify the bulk properties of the Ising ring (for example, the location of the ferromagnet-to-paramagnet QCP).

## 2.2. The quench protocol

We now outline the sudden-quench protocol considered in the present work (see Fig. 1). The Ising ring and the ancillary spins are initially decoupled, i.e., with reference to

Eq. (1), we start with  $\kappa = 0$  and choose the initial state  $|\Psi_0\rangle$  as the ground state of  $\hat{H}_{\mathcal{I}} + \hat{H}_{\mathcal{A}}$ :

$$|\Psi_0\rangle = |\psi_0\rangle \otimes \left( \bigotimes_{i=1}^n |\uparrow\rangle_i \right), \quad (7)$$

where  $|\psi_0\rangle$  is the ground state of the Ising ring and  $\bigotimes_{i=1}^n |\uparrow\rangle_i$  is the vector in the Hilbert space  $\mathcal{H}_{\mathcal{A}} = (\mathbb{C}^2)^n$  with all the  $n$  auxiliary qubits pointing upward along the (3)-direction. At  $t = 0$  the system is suddenly driven out of equilibrium by quenching the parameter  $\kappa$  to a finite value:  $0 \rightarrow \kappa$ , such that  $|\Psi_0\rangle$  is no longer a Hamiltonian eigenstate. Thus for  $t > 0$  the global system evolves nontrivially in real time, according to the usual Schrödinger equation,

$$|\Psi(t)\rangle = e^{-i\hat{H}t} |\Psi_0\rangle, \quad (8)$$

where  $\hat{H}$  is the total Hamiltonian reported in Eq. (1).

In the following discussion, we distinguish between two types of sudden quench: a *soft* quench is related to a tiny change of the parameter  $\kappa$  (decreasing with  $L$ ), so that the system stays close to a quantum transition and thus excites only critical low-energy modes. In contrast, a *hard* quench is not limited by the above condition and typically involves the injection into the system of an extensive amount of energy, in such a way that also *high-energy* excitations are involved.

### 2.3. Decoherence function and energy exchanges

To characterize the scaling properties of the lattice model after the quench, in the different phases and regimes considered, we focus on the coherence and the energetic properties exhibited by the  $n$  ancillary spins (subsystem  $\mathcal{A}$ ).

First of all, we define the decoherence function  $D_{\mathcal{A}}$  as [1]

$$D_{\mathcal{A}}(t) = 1 - \text{Tr}_{\mathcal{A}} [\hat{\rho}_{\mathcal{A}}^2(t)], \quad (9)$$

where  $\hat{\rho}_{\mathcal{A}} \equiv \text{Tr}_{\mathcal{I}} [|\Psi\rangle\langle\Psi|]$  is the reduced density matrix of the external qubits and  $\text{Tr}_{\mathcal{I}/\mathcal{A}}$  represents, respectively, the trace over the Hilbert space of the ring system ( $\mathcal{I}$ ) or that of the probing spins ( $\mathcal{A}$ ). This observable quantifies the coherence properties of  $\mathcal{A}$  and is intimately related to the bipartite entanglement shared by the two distinguished subsystems  $\mathcal{I}$  (blue dots in Fig. 1) and  $\mathcal{A}$  (red dots in Fig. 1) ‡. Namely, it ranges from  $D_{\mathcal{A}} = 0$ , for a pure state, to  $D_{\mathcal{A}} \simeq 1$ , for a maximally entangled state (in the latter case, deviations from the unit value are due to finite Hilbert spaces  $\mathcal{H}_{\mathcal{A}}$ ). By means of the Schmidt decomposition, it is easy to prove that, when the global state  $|\Psi\rangle$  is pure (equivalently, it can be expressed in terms of a single wave function), the decoherence of the system is equal to that of the  $n$  external spins, i.e.  $D_{\mathcal{A}} = D_{\mathcal{I}} \equiv D$ . Here we deal with global pure states, being our global system isolated, therefore from now on we will drop the subscript  $\mathcal{A}$  (or  $\mathcal{I}$ ).

‡ More precisely, the decoherence function  $D$  is strictly connected with the second-order Rényi entropy,  $S_{\mathcal{A}}^{(2)}(t) = -\log \text{Tr}_{\mathcal{A}} [\hat{\rho}_{\mathcal{A}}^2(t)]$ , which is an entanglement monotone.

To address the energy-related and quantum thermodynamic properties of the half-integer monitoring spins, we first define the work statistics distribution  $P(W)$  associated with the quantum quench presented in Sec. 2.2 [38, 39, 1]

$$P(W) = \sum_{m,n} \delta[W - (E_{f,n} - E_{i,m})] |\langle n_f | m_i \rangle|^2 p_{i,m}, \quad (10)$$

where  $\{|m_i\rangle, |n_f\rangle\}$  and  $\{E_{i,m}, E_{f,n}\}$  are the eigenstates and the eigenvalues of, respectively, the starting and the final Hamiltonian (before and after the quench), and  $p_{i,m} = e^{-\beta E_{i,m}}/Z$  is the probability of finding the initial state in the eigenstate  $|m_i\rangle$  of the beginning Hamiltonian, with  $\beta \equiv 1/T$  the inverse temperature and  $Z = \text{Tr}[e^{-\beta \hat{H}}]$  the partition function. At  $T = 0$  we have  $p_{i,0} = 1$  and  $p_{i,\alpha} = 0$ ,  $\forall \alpha > 0$ . The momenta of the work distribution are defined by the integral

$$\langle W^m \rangle \equiv \int dW P(W) W^m. \quad (11)$$

In particular, the first two momenta  $\langle W \rangle, \langle W^2 \rangle$  can be easily addressed by evaluating a static expectation value on the ground state (without the complete knowledge of the whole spectrum), as they have an extremely simple expression in terms of  $\hat{H}_{\mathcal{I}\mathcal{A}}$ :

$$\langle W^m \rangle = \langle \Psi_0 | \hat{H}_{\mathcal{I}\mathcal{A}}^m | \Psi_0 \rangle, \quad \text{if } m = 1, 2. \quad (12)$$

The above relations do not hold for higher momenta of the distribution, with  $m > 2$ . However, given the ground state  $|\Psi_0\rangle$  of Eq. (7), one can easily obtain two simple exact relations for the first two work momenta done on the whole system at the quantum quench:

$$\langle W \rangle = 0, \quad \langle W^2 \rangle = n\kappa^2. \quad (13)$$

After quenching at  $t = 0$ , the energy of the global sunburst system is conserved along the evolution for  $t > 0$ . However, we have significant exchange of energy between the two subsystems. We define the energy-exchange distribution (i.e. the quantum heat) of the qubits associated with two different energy measurements of the subsystem  $\mathcal{A}$ , the first one at  $t = 0$  and the next one at a generic time  $t > 0$  [39, 1],

$$P_{\mathcal{A}}(U, t) \equiv \sum_{n,\alpha} \delta[U - (E_{\mathcal{A}_\alpha} - E_{\mathcal{A}_0})] \left| \langle n, \alpha | e^{-i\hat{H}t} | \Psi_0 \rangle \right|^2, \quad (14)$$

where  $n$  and  $\alpha$  represent, respectively, the energy levels of the ring system and the ones associated with the external spins before the quench. In particular, a simple relation holds for the first momentum  $\langle U \rangle$  of the distribution, i.e.

$$\langle U \rangle(t) = \langle \Psi(t) | \hat{H}_{\mathcal{A}} | \Psi(t) \rangle - \langle \Psi_0 | \hat{H}_{\mathcal{A}} | \Psi_0 \rangle. \quad (15)$$

We remark that the above observable quantifies the average energy stored into the set of  $n$  half-integer spins, as soon as the  $\mathcal{I}$  and  $\mathcal{A}$  subsystems are decoupled at a given time  $t$ . With this respect, the quantum quench protocol we address can be seen, in a different perspective, as the refilling protocol of  $n$  discharged quantum batteries connected to a charger Ising ring system.

### 3. Quantum quenches at the CQT

#### 3.1. Finite number of qubits in the FSS regime

In this section, we present the dynamic FSS framework derived for soft quenches: at  $t = 0$ , the system is suddenly driven out of equilibrium by switching on the coupling  $\kappa$ , such that the global system remains close to a QCP ( $g \approx g_{\mathcal{I}}$ ) and the pairing Hamiltonian  $\hat{H}_{\mathcal{I}\mathcal{A}}$  acts as a small perturbation of  $\hat{H}_{\mathcal{I}} + \hat{H}_{\mathcal{A}}$ . We begin our analysis by keeping the number  $n$  of external qubits fixed in the large- $L$  limit [FSS limit (i)].

As a starting point, we recap some recent FSS results put forward for the equilibrium ground-state properties for the sunburst quantum Ising model [33], in which  $\kappa$  is different from zero and does not depend on time, and then introduce our scaling ansatz required to characterize the various dynamic regimes, basing our arguments on FSS and RG arguments. The natural scaling variable associated with the transverse field strength  $g$  is defined analogously as in the standard quantum Ising model close to the CQT, therefore it reads:

$$G = (g - g_{\mathcal{I}}) L^{y_g}, \quad y_g = 1, \quad (16a)$$

where  $y_g = 1/\nu$  is its RG dimension ( $\nu = 1$  in one dimension). On the basis of energy scales considerations, a common ansatz to provide us with another working scaling variable is given by the ratio of the two relevant low-energy scales  $\delta$ , which characterizes the energy gap of the ancillary qubits close to the critical point, and  $\Delta_{\mathcal{I}}(g_{\mathcal{I}}, L)$ , which represents the finite-size gap of the Ising ring at the QCP. Therefore we consider the scaling variable

$$A = \frac{\delta}{\Delta_{\mathcal{I}}(g_{\mathcal{I}}, L)} \sim \delta L^z, \quad z = 1, \quad (16b)$$

where  $z$  is the dynamic critical exponent. The scaling variable associated with the quench parameter  $\kappa$  is expected to play a role similar to that of a quench generated by Ising symmetry-breaking defects  $\sum_{i=1}^n \hat{D}_i = -\kappa \sum_{i=1}^n \hat{\sigma}_{x=ib}^{(1)}$  at a CQT. For a finite number  $n$  of external spins, the RG dimension of the Hamiltonian parameter  $\kappa$  at the Ising fixed point is given by  $y_{\kappa} = (2 + z - d - \eta)/2 = 7/8$  [40]. Therefore, we define the corresponding scaling variable as [33]

$$K = \kappa L^{y_{\kappa}}, \quad y_{\kappa} = 7/8. \quad (16c)$$

Then, the FSS limit is obtained by taking the large-size limit ( $L \rightarrow \infty$ ), while keeping constant the values of the above mentioned scaling variables  $G, A$ , and  $K$  in Eqs. (16), therefore requiring  $\delta \sim L^{-z}$  and  $\kappa \sim L^{-y_{\kappa}}$ . For instance, a natural ansatz for the scaling behavior of the equilibrium ground-state decoherence function  $D = 1 - \text{Tr}_{\mathcal{A}}[\hat{\rho}_{\mathcal{A}}^2]$  in the FSS limit and close to the CQT of the Ising ring is given by the scaling equation [33]

$$D(n, g, \delta, \kappa, L) \approx \mathcal{D}(n, G, A, K), \quad (17)$$



with  $D(n, g, \delta, 0, L) = \mathcal{D}(n, G, A, 0) = 0$ . Analogous scaling ansatzes can be put forward for other quantities and observables, such as the gap of the global system, the two-point correlation function of the order parameter, as well as its susceptibility, the correlation length, etc ... [33]. These have been carefully verified by means of extensive numerical simulations for finite-size systems in which all the Hamiltonian parameters  $g$ ,  $\delta$ , and  $\kappa$  have been properly rescaled with  $L$  according to the above definitions of scaling variables [33].

We now generalize the above picture to a dynamic scenario, induced by a sudden switch on of the coupling between the ancillary and Ising subsystems, from zero to a nonzero value  $\kappa$ . We consider a soft quench, in such a way that the coupling parameter  $\kappa$  after the quench decreases with  $L$ , keeping the scaling variables  $K$  fixed. In general, dynamic behaviors exhibiting nontrivial time dependences are expected to require another scaling variable associated with the time variable  $t$ , defined as [1]

$$\Theta = t \Delta_{\mathcal{I}}(g_{\mathcal{I}}, L) \sim t L^{-z}, \quad z = 1. \quad (18)$$

The FSS limit for  $L \rightarrow +\infty$  is obtained by keeping constant  $G, A, K$  in Eqs. (16), and also the time variable  $\Theta$  in Eq. (18). Therefore, in this circumstance, we conjecture that observables should generally satisfy universal relations, depending on their scaling dimensions and arguments. For instance, a natural ansatz for the scaling behavior of the decoherence function  $D$  of Eq. (9), in the FSS limit, is given by the scaling equation

$$D(n, g, \delta, \kappa, t, L) \approx \mathcal{D}(n, G, A, K, \Theta), \quad (19)$$

which generalizes Eq. (17) to the dynamic case, by simply adding a further dependence on the time scaling variable  $\Theta$ . We conjecture an analogous scaling ansatz for the average energy  $\langle U \rangle$  stored into the auxiliary qubits [cf. Eq. (15)]:

$$\langle U \rangle(n, g, \delta, \kappa, t, L) \approx L^{-z} \mathcal{E}(n, G, A, K, \Theta), \quad (20)$$

assuming that further analytical contributions are suppressed [1].

As we shall see, the approach to the asymptotic dynamic FSS when keeping  $n$  finite is generally characterized by leading  $O(L^{-7/4})$  corrections. They arise from the analytic expansion of the non-linear scaling field associated with the quench parameter  $\kappa$ , i.e.,  $u_{\kappa} \approx \kappa + c\kappa^3 + \dots$  (where the quadratic term vanishes, due to the symmetric properties of the Ising ring parameter  $\kappa$ ), whose third-order term gives rise to corrections decaying as  $O(L^{-7/4})$  [33]. We also mention that also subleading  $O(L^{-2})$  corrections are generally present in one-dimensional systems with PBC, while systems with boundaries are generally subject to  $O(L^{-1})$  corrections [41].

To verify the above dynamic FSS relations (19) and (20) at the CQT, in Fig. 2 we present some numerical results obtained by means of exact diagonalization and 4<sup>th</sup>-order Runge-Kutta techniques to find the coherent time evolution by integrating the Schrödinger equation in Eq. (8) §. As visible from the nice data collapse of the various

§ We always used a discrete time step of the order of  $\delta t = (1 \div 3) \times 10^{-3}$ . We have checked that the interval  $\delta t$  is sufficiently small to allow us to neglect systematic errors arising from the discretization of the temporal evolution.

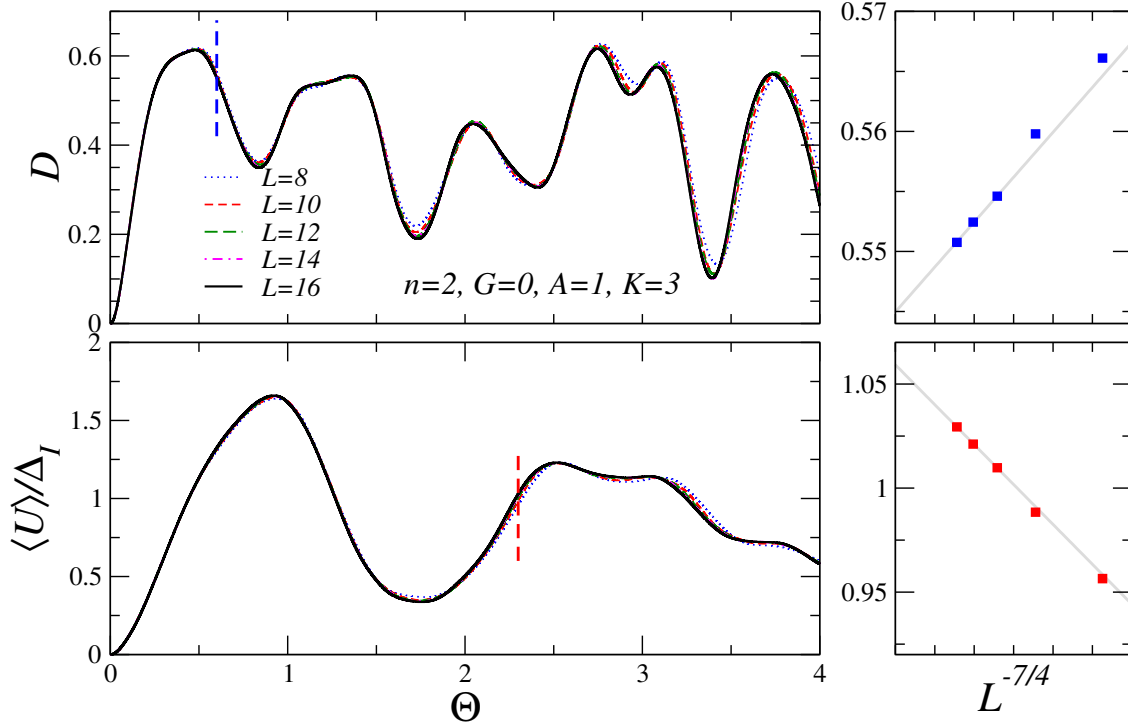


**Figure 2.** Analysis of the decoherence function  $D$  (top panels) and of the rescaled energy stored in the external qubits  $\langle U \rangle / \Delta_I$  (bottom panels) in the FSS limit keeping the number  $n$  of external spins fixed. Left panels: the quantities versus the rescaled time variable  $\Theta$ . The different curves are obtained for various Ising-ring lengths up to  $L = 16$  (and fixed  $n = 2$ ,  $G = 0$ ,  $A = 1$ ,  $K = 3$ ), starting from the initial state  $|\Psi_0\rangle$  of Eq. (7). Right panels: the corresponding scaling corrections for fixed  $\Theta = 0.6$  and  $2.3$ , respectively) are shown to be consistent with a decay  $\sim L^{-7/4}$  (straight lines are drawn to guide to the eye).

curves obtained for different ring lengths  $L$ , the presented results are in agreement with our dynamic FSS theory.

### 3.2. FSS in the large- $n$ limit

It is also interesting to note that, for sufficiently large  $n$ , the dependence on the number of ancillary spins  $n$  can be absorbed into a redefinition of the quench parameter  $K$ , for sufficiently large  $n$ :

$$K' = \sqrt{n} K. \quad (21)$$

Note the large- $n$  limit considered here should be performed after the  $L \rightarrow \infty$  limit. In particular, the quantum model under investigation exhibits appreciable hints of a  $\sqrt{n}$ -law already for relatively small values of  $n \sim 3 \div 5$ , as reported in Fig. 3 for the decoherence function  $D$ . The asymptotic regime appears to be rapidly approached, with  $O(1/n)$  scaling corrections. The square-root dependence on  $n$  of the quench parameter  $K'$  turns out to be the result of the collective (independent) behavior of the ancillary spins, which are indirectly coupled only through the Ising ring. Other observables we

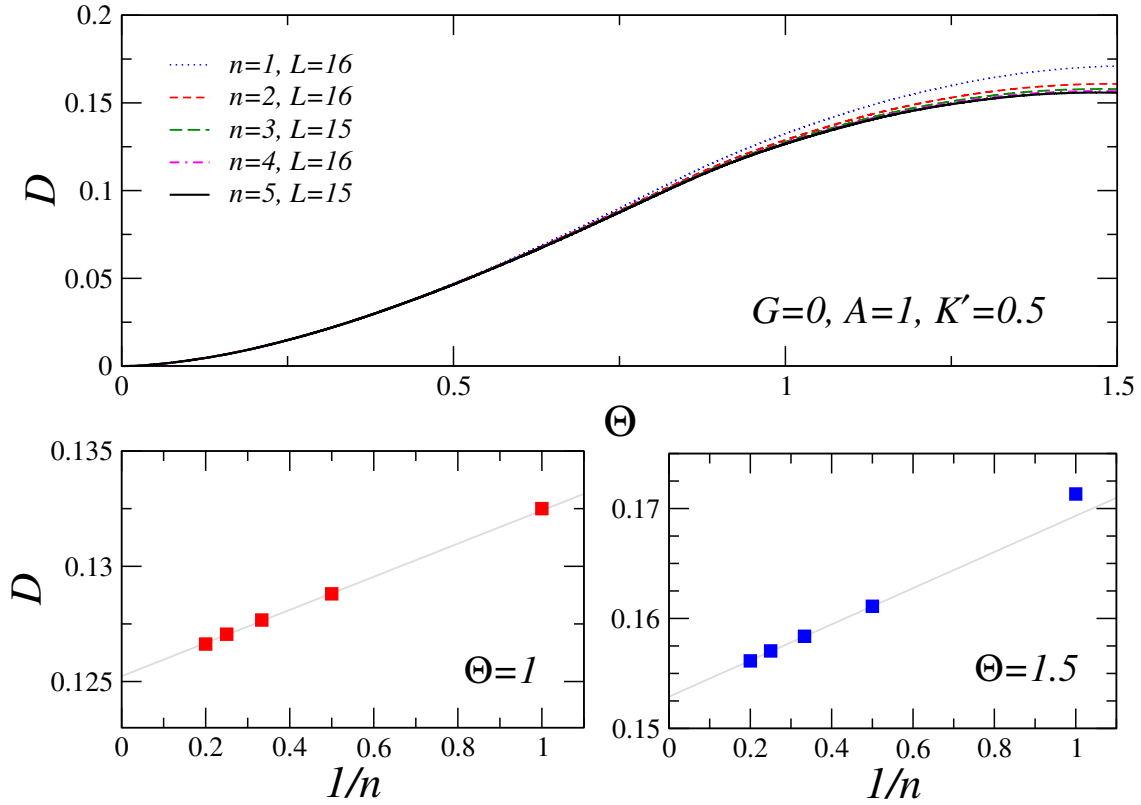


**Figure 3.** Top panel: the decoherence function  $D$  versus  $\Theta$ , for several values of  $n$  at the largest lattice sizes at our disposal, for fixed  $G = 0$ ,  $A = 1$ ,  $K' = 0.5$ . We observe data collapse with increasing  $n$ , within scaling corrections that get asymptotically suppressed as  $n^{-1}$ , as shown for  $\Theta = 1$  (bottom left panel) and  $\Theta = 1.5$  (bottom right panel). We emphasize that each point in the bottom panels is obtained, for fixed  $n$ , by means of large-size extrapolations ( $L \rightarrow \infty$ , at fixed  $n$ ), assuming  $\sim L^{-7/4}$  scaling corrections. Straight lines are drawn to guide to the eye.

have obtained by means of exact diagonalization techniques, as the ratio  $\langle U \rangle / \Delta_{\mathcal{I}}(g_{\mathcal{I}}, L)$ , obey the same large- $n$  FSS relation introduced for  $K'$  (not shown).

### 3.3. Qubits at fixed distance $b$ in the FSS regime

We carry on our discussion by considering the case of soft quenches in which the external spins are placed at fixed distance  $b$  in proximity of a CQT, thus in the large- $n$  limit [FSS limit (ii)]. As working hypothesis, we follow the reasoning for the equilibrium scenario [33] and suppose the theory put forward in the previous section for large  $n$  [in particular, the  $\sqrt{n}$ -law of Eq. (21)] to survive also in this different FSS limit. The most natural guess for the scaling variable associated with the quench strength  $\kappa$  is given in terms of the new scaling variable  $\tilde{K}$ , obtained by replacing  $\sqrt{n} \rightarrow \sqrt{L/b}$  in the definition of  $K'$ , cf. Eq. (21), i.e.

$$\tilde{K} \equiv \sqrt{n} K = \kappa \frac{L^{11/8}}{b^{1/2}}. \quad (22)$$

According to this hypothesis, the previous dynamic FSS relations, cf. Eqs. (19)

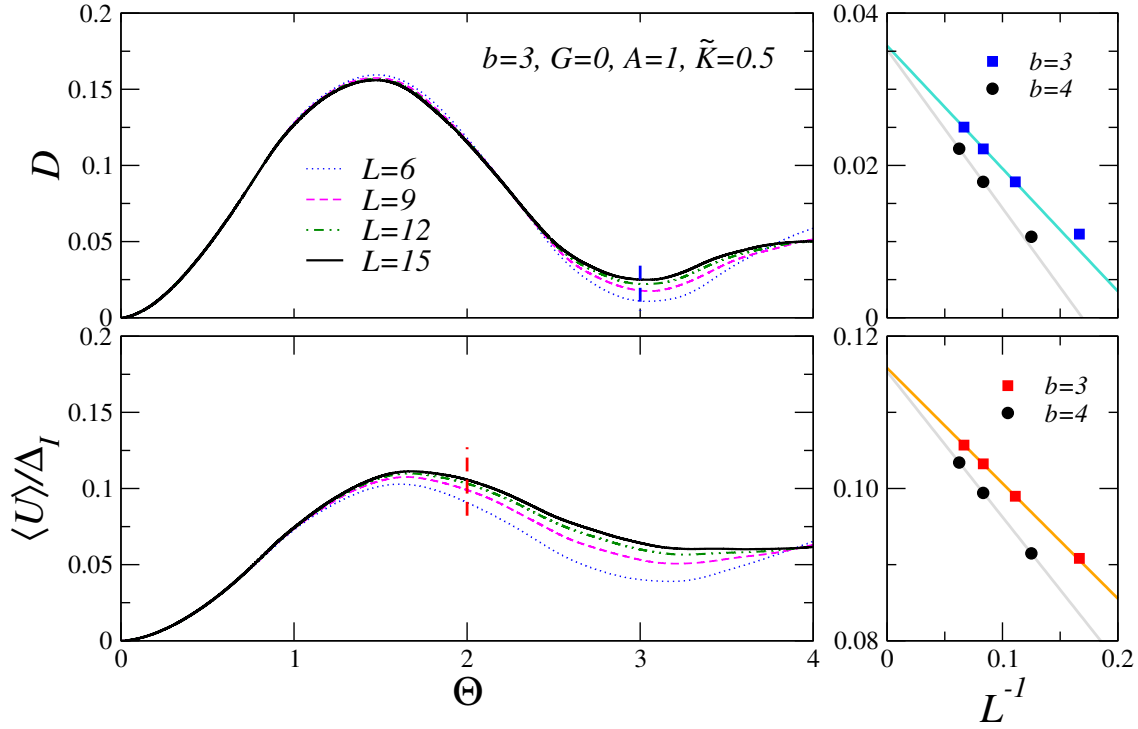


**Figure 4.** Scaling of the decoherence function  $D$  and the RG-invariant ratio  $\langle U \rangle / \Delta_{\mathcal{I}}$  versus  $\Theta$  (top and bottom left panels, respectively), for fixed  $b = 3$  and  $G = 0$ ,  $A = 1$ ,  $\tilde{K} = 0.5$ . Right panels: the corresponding data for  $b = 3$  and  $b = 4$  (not shown on the left), at fixed  $\Theta = 3$  and  $2$  respectively, are consistent with each other, within scaling corrections suppressed as  $\sim L^{-1}$ . Straight lines are drawn to guide the eye.

and (20), should be modified by removing the  $n$  dependence in the corresponding scaling functions and substituting  $K$  with  $\tilde{K}$ . For example, for the decoherence function  $D$ , we conjecture that

$$D(b, g, \delta, \kappa, t, L) \approx \mathcal{D}(A, \tilde{K}, \Theta). \quad (23)$$

Analogous relations are expected to hold also for other observables, as for the energy stored into the monitoring spins  $\langle U \rangle$ . Note that the dependence of  $D$  on  $n$  (which is an extensive energy by definition) is completely encapsulated in the attenuation of the quench intensity  $K$  (being  $\tilde{K}$  fixed in the FSS regime) by a factor  $\sqrt{n} \sim \sqrt{L}$ .

The above conjecture has been verified numerically in Fig. 4, for a fixed distance  $b = 3$  and for  $G = 0$ ,  $A = 1$ , and  $\tilde{K} = 0.5$ . In this figure the decoherence function  $D$ , together with the ratio  $\langle U \rangle / \Delta_{\mathcal{I}}$ , show a nice scaling in terms of the variable  $\Theta$ , thus confirming our hypothesis. We mention that results for  $b = 3$  and  $4$  are consistent with each other, within scaling corrections that decay roughly as  $\sim L^{-1}$ . Such scaling corrections may be related to the  $O(1/n)$  corrections observed in the large- $n$  limit considered in Sec. 3.2, since  $n \sim L$  at fixed  $b$ . To leave the figure easily readable, in the left panels we report the time behavior only for the  $b = 3$  data, however it is worth mentioning that the scaling of the  $b = 4$  data with increasing lattice sizes is very similar to that shown for  $b = 3$ , at all times  $\Theta < 4$ .

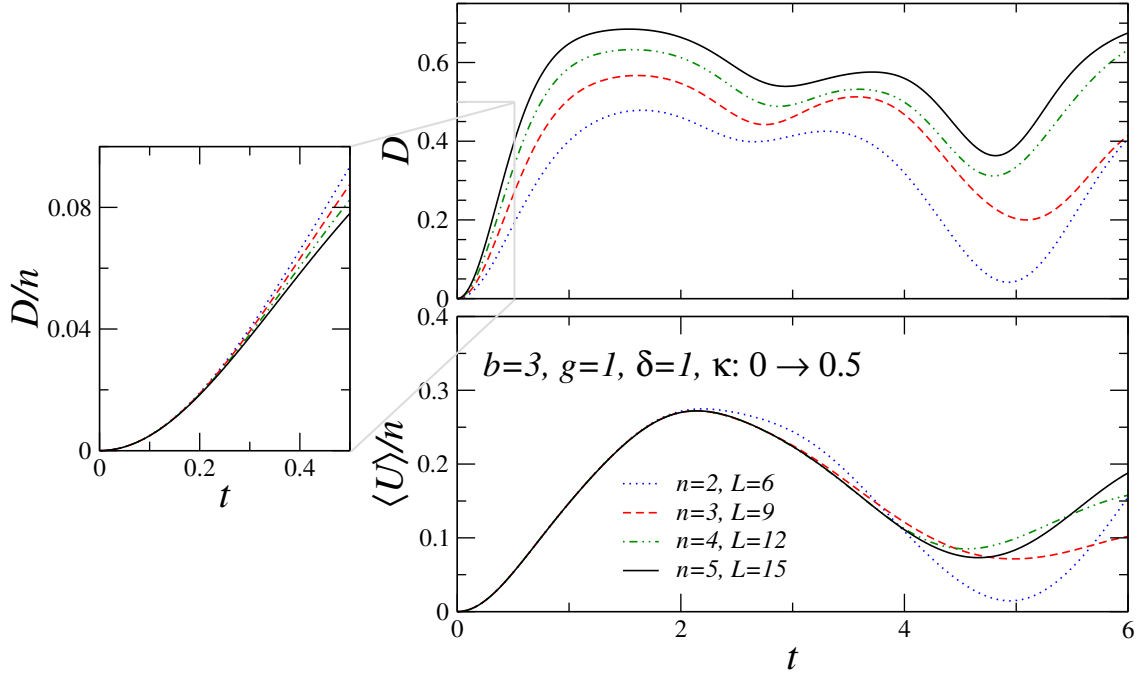


**Figure 5.** Top panel: the decoherence function  $D$  versus  $t$ . Different curves are for various values of  $n$  and  $L$ , while fixing  $b = 3$ , setting  $g = \delta = 1$ , and quenching  $\kappa$  from 0 to 0.5. We note that  $D$  generally increases with  $n$  and, for  $t \ll 1$ , its growth is proportional to the number  $n$  of qubits attached to the ring system, as shown in the inset on the left panel that zooms in on the domain  $t \in [0, 0.5]$  (note that on the y-axis we show  $D/n$ ). Bottom panel: the energy stored per unit qubit  $\langle U \rangle / n$  versus the time  $t$ . The first peak at  $t \approx 2$  is stationary with increasing  $n$ , consistently with an extensive scaling of the energy.

### 3.4. Qubits at fixed distance $b$ and fixed $\delta$

We now consider the dynamics of the quantum Ising ring model, with many independent spins attached, in the hard-quench limit: at  $t = 0$ , the system is suddenly driven out of equilibrium by switching on the coupling  $\kappa$  from zero to a fixed finite value, in such a way that an extensive amount of energy is injected. We fix the spacing distance parameter  $b$  and the excitation energy  $\delta$ , examining different ring lengths  $L$ . Note also that when  $\delta > 0$  the energy scale of the ancillary system is much larger than the gap of the critical Ising ring. In this case, the dynamic FSS frameworks presented in the previous section do not hold anymore, since the hard quench drives the system out of the critical domain. Therefore, the resulting dynamics should be little sensitive to the value  $g$  of the parameter controlling the Ising criticality.

In Fig. 5 we show results for fixed  $g = \delta = 1$  and for a quench intensity  $\kappa : 0 \rightarrow 0.5$ . Differently from the FSS regime analyzed in the previous section, the energy stored per unit qubit is  $\sim O(1)$ , thus scaling extensively with the number of ancillary qubits  $n$  (see the peak in the top panel). For small times  $t \lesssim 0.2$ , we also observe a linear growth with  $n$  in the decoherence function  $D$ , for lattice sizes up to  $L = 15$ .

#### 4. Quantum quenches along the FOQT line

##### 4.1. Finite number of qubits in the FSS regime

We now analyze the model in proximity of the FOQT line ( $g < g_{\mathcal{I}}$ ). For the sake of simplicity, we start from the case with a fixed number  $n$  of ancillary spins [FSS limit (i)]. We stress again that, in the FSS and thermodynamic limit, a finite number of external spins cannot change the bulk properties of the ring system, and in particular its equilibrium quantum phases. To begin with, we present the scaling variables employed across this section to derive dynamic FSS relations for quantum quenches at FOQTs.

Still relying our FSS arguments on the basis of the relevant energy scales associated with each subsystem, we can first introduce the analogue of the scaling variables (16b) and (16c) for systems close to FOQTs, in the static case. Namely, we define the variable [33, 1]

$$Y_{\delta} = \frac{\delta}{\Delta_{\mathcal{I}}(g, L)}, \quad (24a)$$

as the ratio between the energy of the elementary excitation of a single qubit and the gap of the finite-size Ising ring  $\Delta_{\mathcal{I}}(g, L)$  at size  $L$  and for a transverse field  $g < g_{\mathcal{I}}$ . Similarly to Ising models at the FOQT driven by a longitudinal magnetic field, we may also introduce the scaling variable  $Y_{\kappa}$  associated with the variable  $\kappa$ , [33, 36]

$$Y_{\kappa} = \frac{\kappa}{\Delta_{\mathcal{I}}(g, L)}, \quad (24b)$$

which determines the *softness* of the quantum quench. To extend the FSS framework to the dynamic scenario, a further scaling variable associated to the time  $t$  is required, analogously as was done in Eq. (18). Namely, [34]

$$\Theta = t \Delta_{\mathcal{I}}(g, L), \quad (25)$$

where  $\Delta_{\mathcal{I}}(g, L)$  now denotes the gap of the Ising-ring system for  $g < g_{\mathcal{I}}$ . Therefore, differently from CQTs in the FSS limit, data collapse of observables at FOQTs is expected to be recovered at time scales that substantially depend on the way in which the gap  $\Delta_{\mathcal{I}}$  closes with  $L$ : generally, these may range from power-law to exponentially large times, according to the different boundary conditions [1]. In our specific case with a PBC geometry, we expect an exponential scaling  $\Delta_{\mathcal{I}}(g < g_{\mathcal{I}}, L) \propto g^L$ .

Relations analogous to those presented at the CQTs are still formally valid in proximity of FOQTs, after properly replacing the corresponding scaling variables. For example, the dynamic FSS relations related to the decoherence function  $D$  [cf. Eq. (19), for systems close to the CQT] is now expected to scale as

$$D(n, g, \delta, \kappa, t, L) \approx \mathcal{D}(n, g, Y_{\delta}, Y_{\kappa}, \Theta), \quad (26a)$$

while the energy stored into the auxiliary qubits [cf. Eq. (20) at the CQT] should read

$$\langle U \rangle (n, g, \delta, \kappa, t, L) \approx \Delta_{\mathcal{I}}(g, L) \mathcal{E}(n, g, Y_{\delta}, Y_{\kappa}, \Theta). \quad (26b)$$

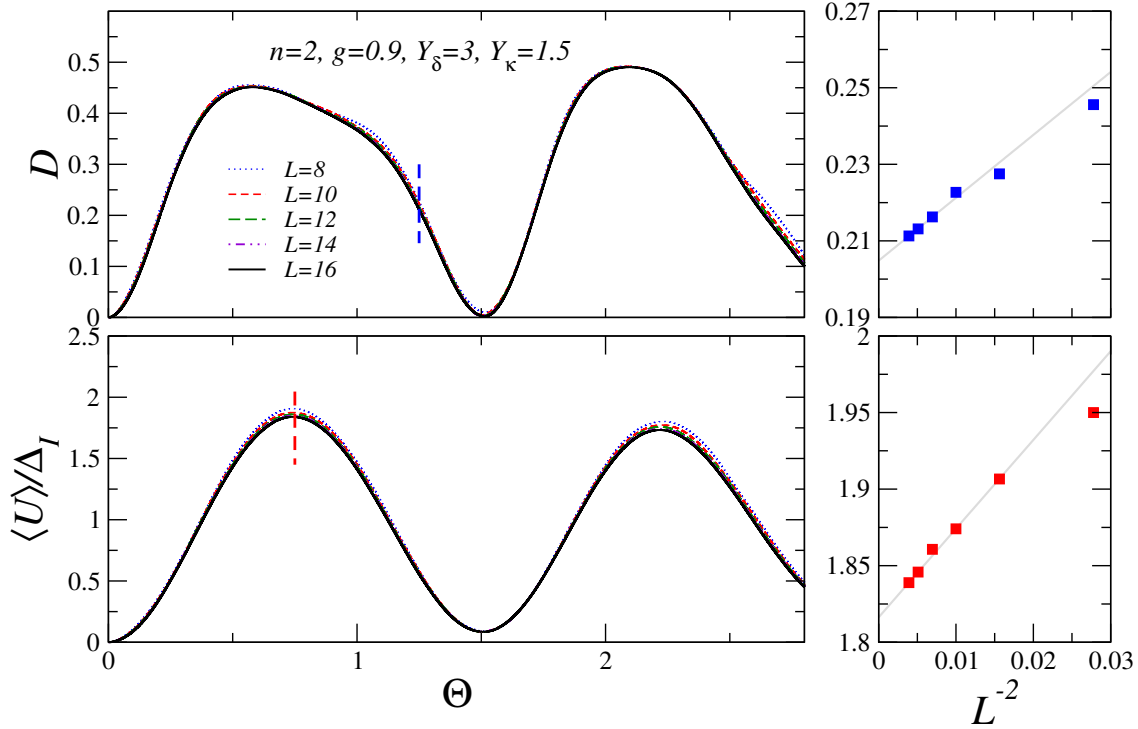


**Figure 6.** Top left panel: the decoherence function  $D$  in terms of the rescaled time  $\Theta$  at the FOQT for  $g = 0.9$ , with  $Y_\delta = 3, Y_\kappa = 1.5$ , and for fixed  $n = 2$ . Bottom left panel: the ratio  $\langle U \rangle / \Delta_I$  versus  $\Theta$ . In the corresponding right panels we report the same data as a function of  $L$ , for fixed  $\Theta = 1.25$  and  $0.75$ , showing that scaling corrections are substantially consistent with a decay  $\sim L^{-2}$ . Straight lines are drawn to guide the eye.

The analogous counterparts for static conditions with a constant and finite  $\kappa$  (i.e., without time dependence induced by changes of the parameter  $\kappa$ ) have been numerically verified in Ref. [33]. Here we rather focus on numerically testing our above dynamic FSS framework for soft quenches close to the FOQT line  $g < g_{\mathcal{I}}$ .

Specifically, the dynamic FSS laws in Eqs. (26) for systems close to FOQTs are supported by the data in Fig. 6, which shows an excellent data collapse for the various curves at different ring sizes  $L$ , and for rescaled times smaller than  $\Theta < 2.8$  (left panels). Scaling corrections appear to be suppressed roughly as  $\sim L^{-2}$ , with increasing  $L$  (right panels). We have checked that the above FSS predictions are verified numerically also for a different value of  $g = 0.8$ , by considering the case for fixed  $n = 2$  and ring sizes up to  $L = 12$  (not shown).

Also at FOQTs we observed that the dependence of observables on the number of ancillary spins could be absorbed into a redefinition of the variable  $Y_\kappa$  as

$$Y'_\kappa = \sqrt{n} Y_\kappa. \quad (27)$$

To this extent, in Fig. 7 we present result for the decoherence function  $D$  for the largest lattice sizes at our disposal, for several values of  $n$ . For fixed  $\Theta = 0.5$  (bottom left)

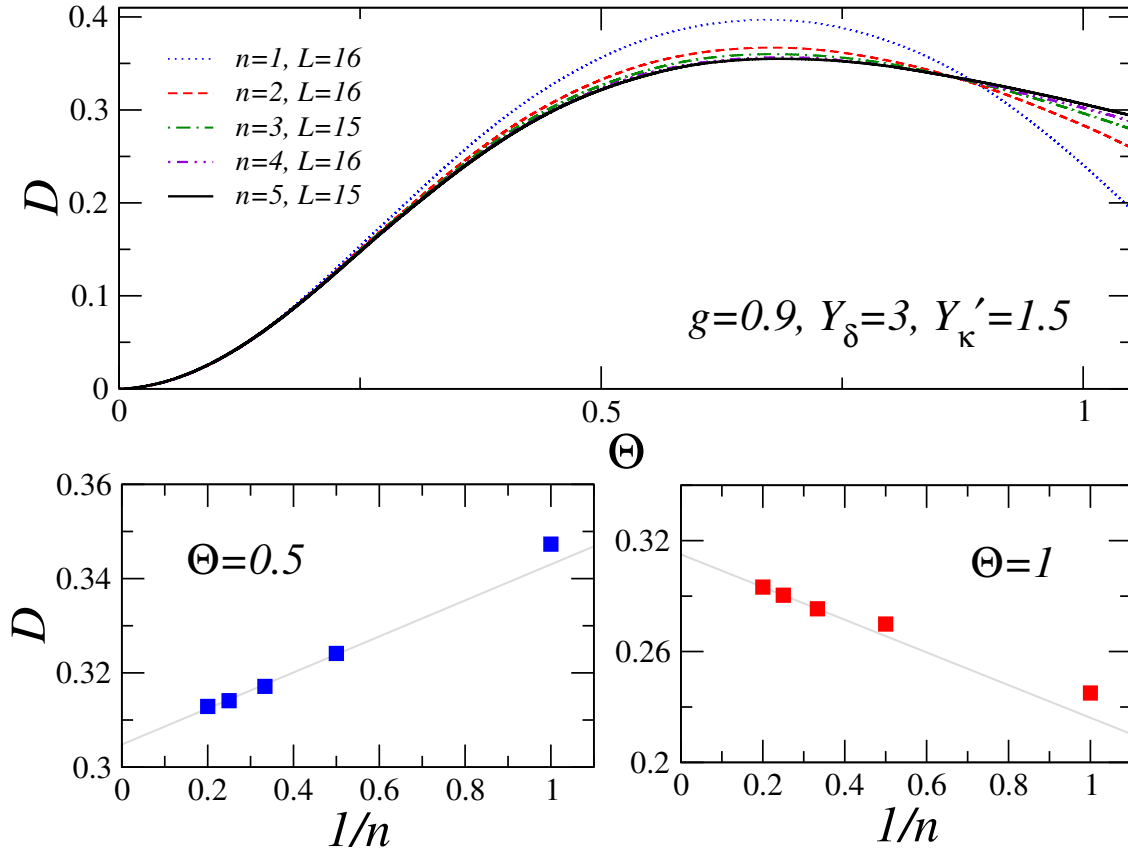


**Figure 7.** Top panel: the decoherence function  $D$  versus  $\Theta$ , for several values of  $n = 1, \dots, 5$  for the largest lattice sizes available with our exact diagonalization methods. Scaling corrections at  $\Theta = 0.5$  (bottom left panel) and 1 (bottom right panel) are consistent with a decay  $\sim L^{-1}$ . Straight lines are drawn to guide the eye. Here we stay close to the FOQT at  $g = 0.9$ , fixing  $Y_\delta = 3$  and  $Y'_\kappa = 1.5$ .

and  $\Theta = 1$  (bottom right panel) we observe a power-law convergence in the number of external spins as  $\sim n^{-1}$  ||.

#### 4.2. Qubits at fixed distance $b$ in the FSS regime

Following the results carried out in the previous section, we now extend our dynamic FSS framework at FOQTs to the domain when  $b$  is fixed, thus the number of quantum probes increases with the ring size  $L$  [FSS limit (ii)]. In this limit, analogously to what was done in Eq. (22) close to a CQT, we recognize as a relevant scaling variable for the quench intensity the ratio [33]

$$\tilde{Y}_K = \sqrt{n} Y_K = \frac{\kappa L^{1/2}}{\Delta_{\mathcal{I}}(g, L) b^{1/2}}. \quad (28)$$

With reference to the previous section, dynamic FSS relations can be obtained by replacing  $Y_K$  with  $\tilde{Y}_K$ , e.g., in Eqs. (26). Our scaling hypotheses are checked numerically

|| For each  $n$ , we have performed large-size extrapolations assuming  $L^{-2}$  scaling corrections, by fitting an ansatz function  $D(L) = a + b/L^2$



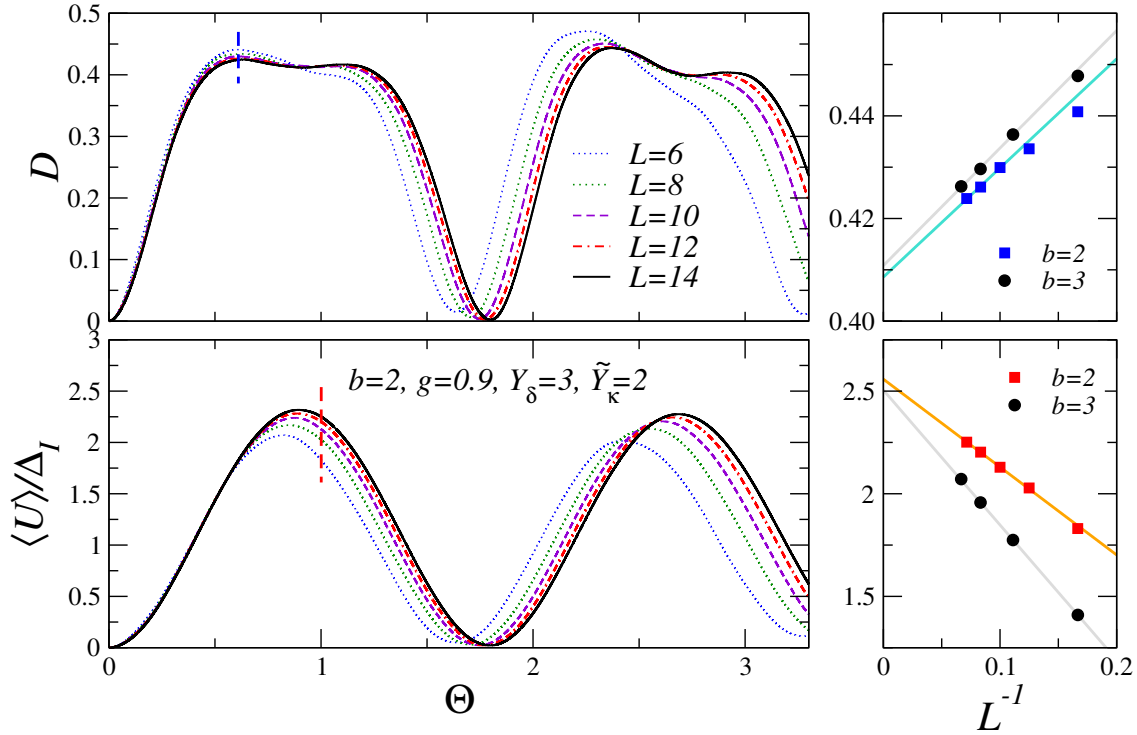


**Figure 8.** Top panels: the decoherence function  $D$  versus the rescaled time  $\Theta$  (left) and the inverse size (right). Bottom panels: same as in the top panels, but for the stored energy  $\langle U \rangle$  rescaled with the gap  $\Delta_{\mathcal{I}}(g = 0.9, L)$  of the finite-size Ising ring. The scaling corrections shown in the right panels, evaluated for the top and bottom panels respectively at  $\Theta = 0.6$  and  $1$ , are in good agreement with a decay  $L^{-1}$  (straight lines are drawn to guide the eye). We fix  $g = 0.9$ ,  $b = 2$ , and  $Y_{\delta} = 3$ ,  $\tilde{Y}_{\kappa} = 2$ . However, similarly to Fig. 4, in the insets we also show some data associated with a different value of  $b = 3$ , to emphasize the independence of the observables on  $b$  in the large  $L$  limit, while keeping  $\tilde{Y}_{\kappa} = \kappa L^{1/2}/[b^{1/2}\Delta_{\mathcal{I}}(g, L)]$  fixed.

in Fig. 8 for lattice sizes up to  $L = 14$ , within scaling corrections that appear to decay as  $\sim L^{-1}$ , which should be again related to the  $O(1/n)$  corrections found in the large- $n$  limit at fixed  $n$ .

We skip the discussion of the hard-quench limit starting from the ferromagnetic phase with  $g < g_{\mathcal{I}}$ , since we do not find any relevant difference to that found when performing the quench from the QCP. In the zero-temperature equilibrium phase diagram of the sunburst quantum Ising model, it was indeed conjectured that, when  $b$  is fixed, the critical line characterizing the breaking of the  $\mathbb{Z}_2$  global symmetry shifts to higher values  $g_c(\kappa) > g_{\mathcal{I}}$  for any  $\kappa \neq 0$  [33]. Since the hard-quench protocol we consider always pushes the system away from criticality into the ordered phase, we do not find any remarkable difference between quenches performed when  $g < g_{\mathcal{I}}$  or  $g = g_{\mathcal{I}}$ .

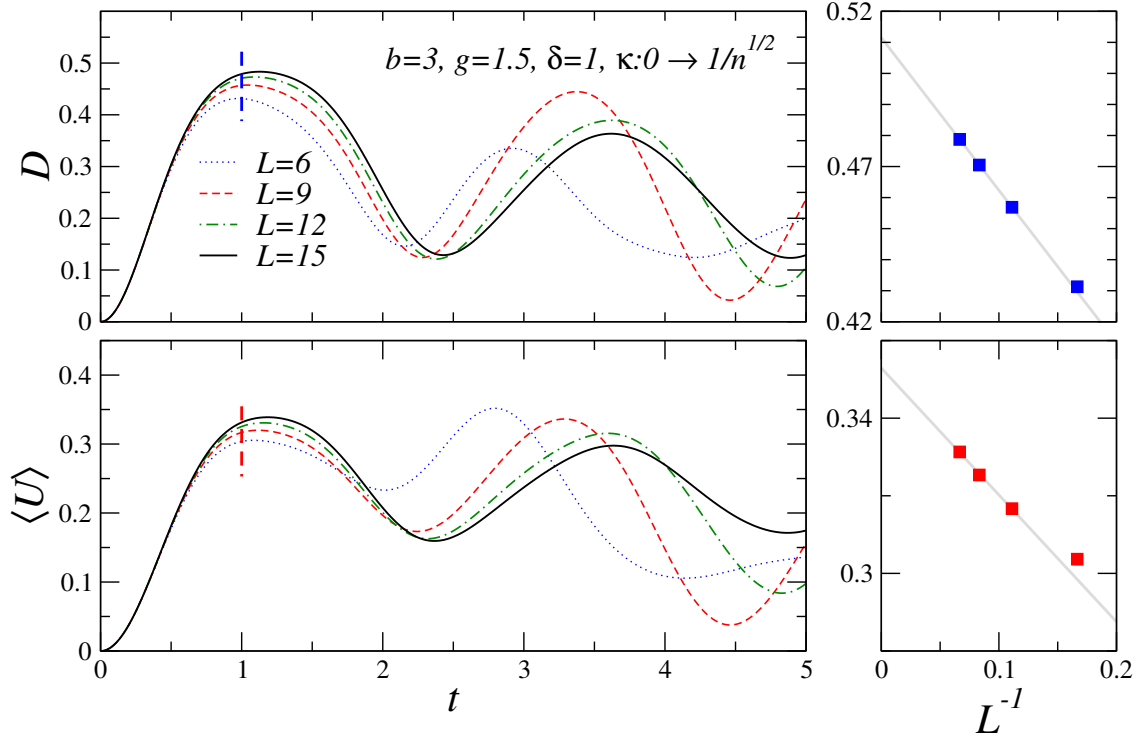


**Figure 9.** Results for quantum quenches starting from the disordered phase. We keep  $b = 3, g = 1.5, \delta = 1$  fixed, and rescale the intensity of the quench with  $n$ , such that  $\kappa : 0 \rightarrow 1/\sqrt{n}$ . Top left panel: the decoherence function  $D$  versus  $t$ . Bottom left panel: the energy  $\langle U \rangle \propto n$  stored into the ancillary qubits versus  $t$ . Scaling corrections, shown in the corresponding right panels for  $t = 1$ , are consistent with a decay  $\sim L^{-1}$  (straight lines are drawn to guide the eye).

## 5. Quantum quenches from the disordered phase

Let us now present some numerical results for the dynamics of our lattice system, when it is driven out of equilibrium from the disordered phase ( $g > g_I$ ), fixing the distance  $b$  between two consecutive external spins. Guided by the  $\sqrt{n}$ -behavior put forward in the dynamic FSS at CQTs and FOQTs, and by the equilibrium properties of the sunburst quantum Ising model [33], we first address the dynamics of the system in the disordered phase with rescaled quench intensity  $\kappa : 0 \rightarrow 1/\sqrt{n}$ .

In Fig. 9 we present results for fixed  $g = 1.5$  and  $\delta = 1$ . We remember the reader that the typical fluctuations associated with the global work done on the overall system at the quench scale as  $\sqrt{\langle W^2 \rangle} = \kappa \sqrt{n}$ , so that it remains constant in this limit. Therefore, in this regime, the coupling between the ring and the external spins decreases as the lattice size increases. Our results suggest that, for small times  $t \lesssim 1$ , the peak of both the decoherence function  $D$  and the energy stored into the probes  $\langle U \rangle$  approach a constant behavior for large  $L$  (note that the latter quantity increases linearly with the lattice size  $\langle U \rangle \propto n \langle \hat{\Sigma}^{(3)} \rangle$ ). We also present some results for fixed quench intensity  $\kappa$  and  $g = 1.5$  in Fig. 10. As expected, in this second case, the decoherence function  $D$  generally increases with the number  $n$  of external spins (at small times it depends

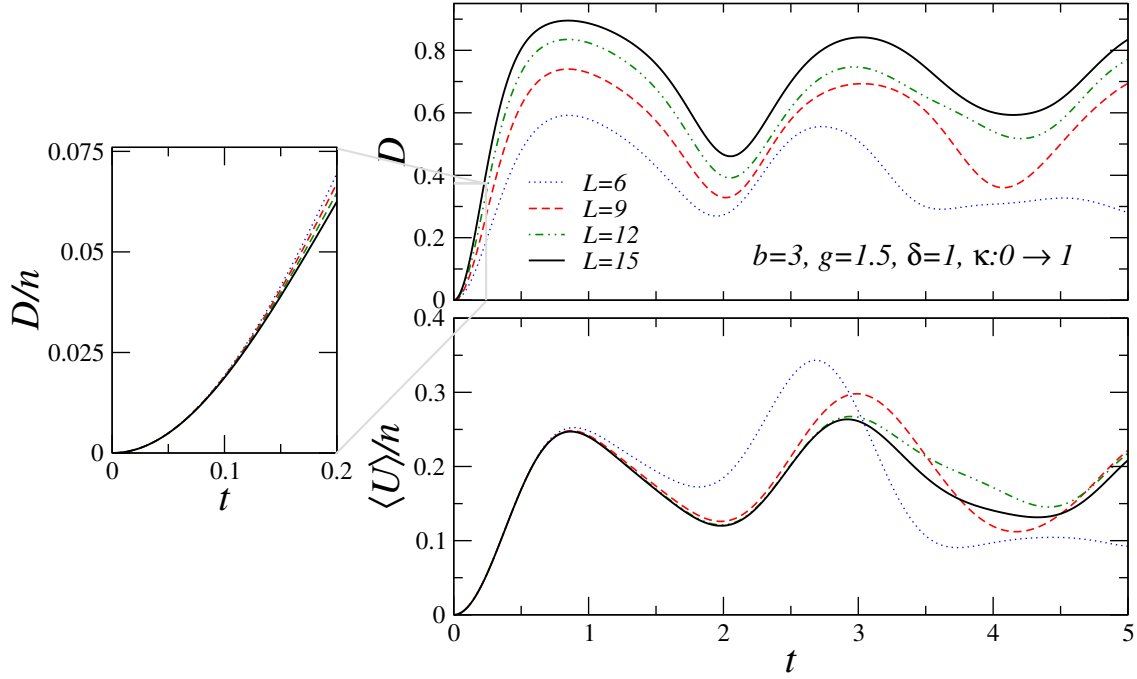


**Figure 10.** Results for quantum quenches starting from the disordered phase ( $g = 1.5$ ). We maintain fixed  $b = 3$ ,  $\delta = 1$  and perform a quench for  $\kappa : 0 \rightarrow 1$ . The decoherence function generally increases with increasing the number of ancillary spins  $n$ . The inset shows that such function increases linearly with  $n$  at small times  $t \lesssim 0.2$ . Bottom panel: The maximum energy per unit spin encapsulated in the external qubits is roughly independent of  $n$ .

on  $n$  as  $D \propto n$ , as shown in the correspondent inset) and the first peak of  $\langle U \rangle$  scales extensively with the number of ancillaries.

## 6. Quenches with Ising ring of fixed length

Finally, we analyze some examples of hard quenches when the length  $L$  of the Ising ring is fixed, but the number of external probes vary, which is perhaps the most relevant case for quantum-metrology purposes or for setting a hypothetical quantum-battery device. To this extent, the focus is on the role of  $n$  in determining the dynamics of observables (in particular the energy  $\langle U \rangle$ ) when the ancillary qubits which probe the ring are independent from each other. To remark this fact, we compare our results with the analogous ones obtained by coupling consecutive nearest-neighbor external qubits along the transverse direction. As an exploratory study, we consider the following extension of the ancillary Hamiltonian (3)

$$\hat{H}'_{\mathcal{A}} = \hat{H}_{\mathcal{A}} - J_{\Sigma} \sum_{i=1}^n \hat{\Sigma}_i^{(3)} \hat{\Sigma}_{i+1}^{(3)}, \quad (29)$$

where PBC are intended in the second term, thus preserving the translational invariance of the lattice model, modulo  $b$ . In the following we present some results for the case

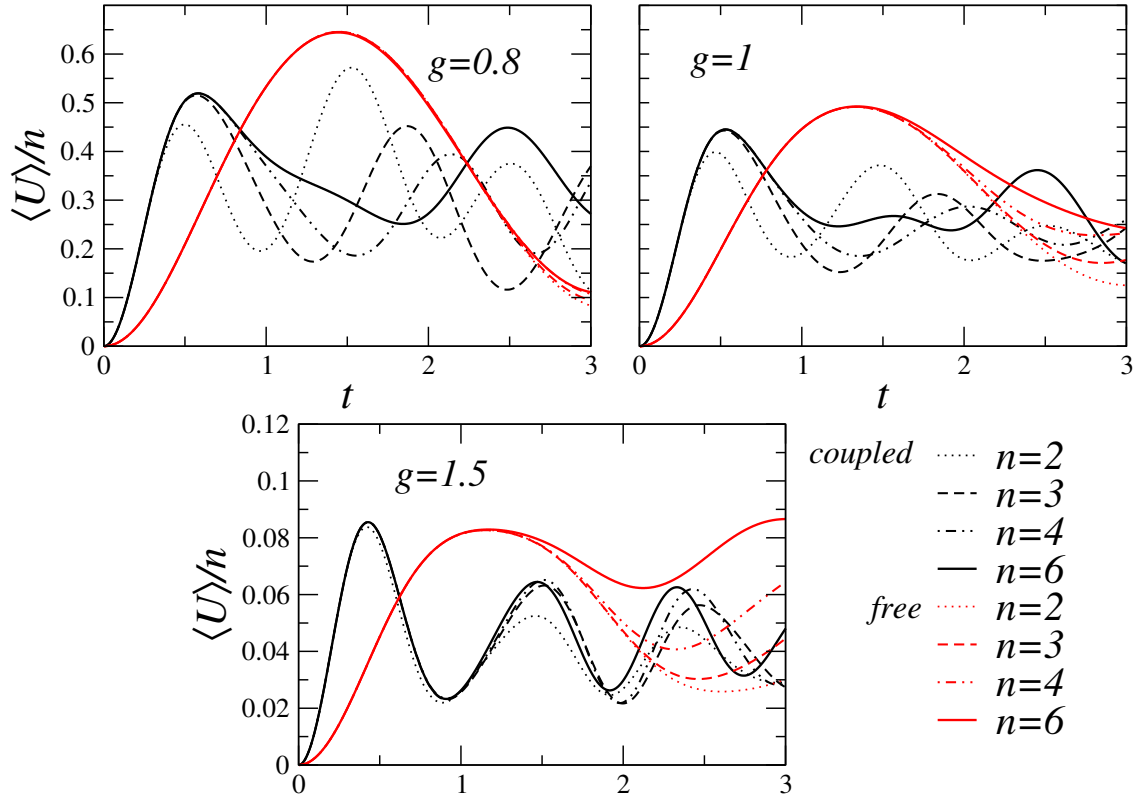


**Figure 11.** The average energy per unit spin stored into an external qubit versus the time  $t$ , for both cases of independent external spins (*free* in the legend) and of external spins which interact according to Eq. (29) (*coupled* in the legend). Here we consider  $L = 12$  and vary  $n$  as indicated in the legend, fix  $\delta = 1$ , and perform a quench of  $\kappa$  from 0 to 1 for several values of  $g$ . There is no striking difference between the two quenches shown at  $g = 0.8$  and 1: the *free* and the *coupled* model can absorb roughly the same amount of energy  $\langle U \rangle / n \approx 0.5$ . The capability of energy absorption worsen in both models for  $g = 1.5$  (note that the  $y$  scale in the last graph is different from the upper panels).

$J_\Sigma = 1$ .

Note that the pre-quench state  $|\Psi_0\rangle$  in Eq. (7) is still the ground state of the global system with  $\kappa = 0$ , independently of the presence of the new interaction term of Eq. (29). Of course, the post-quench unitary dynamics will change, and thus also the average energy stored into the qubits:

$$\langle U \rangle = \langle \Psi(t) | \hat{H}'_{\mathcal{A}} | \Psi(t) \rangle - \langle \Psi_0 | \hat{H}'_{\mathcal{A}} | \Psi_0 \rangle. \quad (30)$$

In Fig. 11 we present some results for fixed  $\delta = 1$ , quench intensity  $\kappa : 0 \rightarrow 1$  and ring length  $L = 12$  (which offers several combinations of  $b$ , commensurate to the ring length) to be investigated. Looking at the peaks in the energy stored for all the three values of the coupling  $g$  we have considered, each one representing a different phase of the Ising ring, we first note an extensive scaling of the energy with the number  $n$  of qubits: In particular, the maximum energy stored into a single spin is roughly the same for  $g = 0.8$  and 1,  $\langle U \rangle / n \approx 0.45 \div 0.50$ , whereas it appears strongly suppressed to

$\langle U \rangle / n \approx 0.08$  for both models, when  $g = 1.5$ ). However, it is also worth noting that the charging of the qubits that are *coupled* is generally significantly faster than that obtained when the external qubits are independent from each other. This last fact holds for all values of  $g$  shown in Fig. 11, as well as the extensiveness with  $n$  of the energy stored  $\langle U \rangle$ . We have not found evidence of striking differences between the energy stored into the probing apparatus of the two models. However, we should say that we have not done an extended study of the optimal parameters in this respect.

## 7. Summary and conclusions

We have studied the post-quench unitary dynamics of an ensemble of quantum spin-1/2 objects arranged in a sunburst geometry: namely, at a given reference time, some of the  $L$  spins of a transverse-field quantum Ising ring are suddenly and locally coupled to a set of  $n$  independent external qubits ( $n \leq L$ ), along the longitudinal direction, in such a way to maintain a residual translation invariance and the Ising  $\mathbb{Z}_2$  symmetry. The system exhibits various quantum phases separated by first order (FOQTs) or continuous (CQTs) quantum transitions, which are controlled by the various Hamiltonian parameters as the Ising transverse field  $g$ , the energy scale  $\delta$  of the external qubits, and the interaction strength  $\kappa$  between the two subsystems [33]. This scenario represents a useful playground where to study the mutual interplay and the properties of different subparts of a complex quantum many-body system, such as the onset of decoherence or the exchange of heat and work between them. In particular, the set of  $n$  qubits can be interpreted as a probing apparatus ( $\mathcal{A}$ ) for the set of  $L$  spins composing the Ising ring ( $\mathcal{I}$ ).

By using proper dynamic FSS frameworks [1] we show that, at the Ising CQT ( $g = g_{\mathcal{I}}$ ) or along its FOQT line ( $|g| < g_{\mathcal{I}}$ ), peculiar dynamic scaling regimes may appear. To this purpose, we explicitly consider two different large-size limits where dynamic FSS laws emerge: we allow  $L \rightarrow \infty$  while fixing either the number  $n$  of external qubits, or their nearest-neighbor interspace distance  $b$ . For a sufficiently large number  $n$  of external spins, the dependence of observables on the number  $n$  of qubits can be reabsorbed into a redefinition of the quench parameter, by replacing the scaling variable associated with  $\kappa$  with  $\sqrt{n} \kappa$ .

We also consider quenches within the Ising-disordered phase ( $g > g_{\mathcal{I}}$ ), addressing the role of the  $\sqrt{n}$ -behavior out of the FSS framework. We observe that, by maintaining  $\kappa\sqrt{n}$  fixed, which represents the typical energy scale of work done on the whole system [in particular  $\sqrt{\langle W^2 \rangle} = \kappa\sqrt{n}$ , cf. Eq. (13)], several quantities that are expected to scale extensively with  $n$  approach a constant value in the large  $L$  limit. In other words, our results suggest that even beyond the FSS regime, there is a fair tradeoff between the *linear* enlargement of both the Ising ring and ancillary spins (they both increase with  $L$  when  $b$  is fixed) and the  $\sqrt{n}$ -reduction of the quench intensity.

Finally, we compare our results to those obtained when also a nearest-neighbor coupling among the external qubits is taken into account, maintaining the Ising-ring length fixed. For quenches with  $\kappa : 0 \rightarrow 1$ , no substantial differences emerge between

the two lattice models: although the recharging of the *coupled* model is faster than that of the *free* system, the two models can roughly store the same amount of energy. However, our study was only exploratory, we have not done a through optimization study of the model parameters.

Our dynamic framework has been carefully tested by means of numerical exact diagonalization techniques on systems with only  $\sim O(20)$  quantum spins. Moreover, results for the time behavior of the decoherence function are strictly connected with the experimentally measurable Rényi entropy [42, 43], while the average energy stored into the external qubits may represent a central thermodynamic quantity to be monitored in the study of quantum-battery devices [9]. The reduced number of spins in our simulated systems suggests that quantum simulators with existing technology should be able to access our predictions, e.g., by using trapped ions [44], ultracold atoms [45, 10], or superconducting qubits [46, 47].

## References

- [1] Rossini D and Vicari E, *Coherent and dissipative dynamics at quantum phase transitions*, 2021 *Phys. Rep.* **936** 1
- [2] Dziarmaga J, *Dynamics of a quantum phase transition and relaxation to a steady state*, 2010 *Adv. Phys.* **59** 1063
- [3] Polkovnikov A, Sengupta K, Silva A and Vengalattore M, *Colloquium: Nonequilibrium dynamics of closed interacting quantum systems*, 2011 *Rev. Mod. Phys.* **83** 863
- [4] Georgescu I M, Ashhab S and Nori F, *Quantum Simulation*, 2014 *Rev. Mod. Phys.* **86** 154
- [5] Nielsen M A and Chuang I L, *Quantum Computation and Quantum Information*, 2010 (Cambridge University Press, Cambridge)
- [6] Lambert N, Chen Y-N, Cheng Y-C, Li C M, Chen G Y and Nori F, *Quantum biology*, 2013 *Nat. Phys.* **9** 10
- [7] Goold J, Huber M, Riera A, del Rio L and Skrzypczyk P, *The role of quantum information in thermodynamics*, 2016 *J. Phys. A: Math. Theor.* **49** 143001
- [8] Vinjanampathy S and Anders J, *Quantum Thermodynamics*, 2016 *Contemp. Phys.* **57** 545
- [9] Campaioli F, Pollock F A and Vinjanampathy S, in *Thermodynamics in the Quantum Regime*, edited by Binder F, Correa L A, Gogolin C, Anders J and Adesso G, 2018 (Springer, New York), pp. 207–225
- [10] Schäfer F, Fukuhara T, Sugawa S, Takasu Y and Takahashi Y, *Tools for quantum simulation with ultracold atoms in optical lattices*, 2020 *Nat. Rev. Phys.* **2** 411
- [11] Bloch I, Dalibard, J and Zwerger W, *Many-body physics with ultracold gases*, 2008 *Rev. Mod. Phys.* **80** 885
- [12] Zurek W H, *Decoherence, einselection, and the quantum origins of the classical*, 2003 *Rev. Mod. Phys.* **75** 715
- [13] Zurek W H, *Environment-induced superselection rules*, 1982 *Phys. Rev. D* **26** 1862
- [14] Hutton A and Bose S, *Mediated entanglement and correlations in a star network of interacting spins*, 2004 *Phys. Rev. A* **69** 042312
- [15] Cucchietti F M, Paz J P and Zurek W H, *Decoherence from spin environments*, 2005 *Phys. Rev. A* **72** 052113
- [16] Quan H T, Song Z, Liu X F, Zanardi P and Sun C P, *Decay of Loschmidt Echo Enhanced by Quantum Criticality*, 2006 *Phys. Rev. Lett.* **96** 140604
- [17] Rossini D, Calarco T, Giovannetti V, Montangero S and Fazio R, *Decoherence induced by interacting quantum spin baths*, 2007 *Phys. Rev. A* **75** 032333

- [18] Cucchietti F M, Fernandez-Vidal S and Paz J P, *Universal decoherence induced by an environmental quantum phase transition*, 2007 *Phys. Rev. A* **75** 032337
- [19] Bortz M and Stolze J, *Exact dynamics in the inhomogeneous central-spin model*, 2007 *Phys. Rev. B* **76** 014304
- [20] Cormick C and Paz J P, *Decoherence induced by a dynamic spin environment: The universal regime*, 2008 *Phys. Rev. A* **77** 022317
- [21] Zurek W H, *Quantum Darwinism*, 2009 *Nat. Phys.* **5** 181
- [22] Damski B, Quan H T and Zurek W H, *Critical dynamics of decoherence*, 2011 *Phys. Rev. A* **83** 062104
- [23] Nag T, Divakaran U and Dutta A, *Scaling of the decoherence factor of a qubit coupled to a spin chain driven across quantum critical points*, 2012 *Phys. Rev. B* **86** 020401(R)
- [24] Suzuki S, Nag T and Dutta A, *Dynamics of decoherence: Universal scaling of the decoherence factor*, 2016 *Phys. Rev. A* **93** 012112
- [25] Vicari E, *Decoherence dynamics of qubits coupled to systems at quantum transitions*, 2018 *Phys. Rev. A* **98** 052127
- [26] Fiorelli E, Cuccoli A and Verrucchi P, *Critical slowing down and entanglement protection*, 2019 *Phys. Rev. A* **100** 032123
- [27] Rossini D and Vicari E, *Scaling of decoherence and energy flow in interacting quantum many-body systems*, 2019 *Phys. Rev. A* **99** 052113
- [28] Ashida Y, Shi T, Schmidt R, Sadeghpour H R, Cirac J I and Demler E, *Quantum Rydberg Central Spin Model*, 2019 *Phys. Rev. Lett.* **123** 183001
- [29] Villazon T, Claeys P W, Pandey M, Polkovnikov A and Chandran A, *Persistent dark states in anisotropic central spin models*, 2020 *Sci. Rep.* **10** 16080
- [30] Liu J, Shi H, Shi Y, Wang X and Yang W, *Entanglement and work extraction in the central-spin quantum battery*, 2021 *Phys. Rev. B* **104** 245418
- [31] Arisoy O and Müstecaplıoğlu Ö E, *Few-qubit quantum refrigerator for cooling a multi-qubit system*, 2021 *Sci. Rep.* **11** 12981
- [32] Niknam M, Santos L F and Cory D G, *Experimental Detection of the Correlation Rényi Entropy in the Central Spin Model*, 2021 *Phys. Rev. Lett.* **127** 080401
- [33] Franchi A, Rossini D and Vicari E, *Quantum many-body spin rings coupled to ancillary spins: The sunburst quantum Ising model*, 2022 arXiv:2202.07999
- [34] Pelissetto A, Rossini D and Vicari E, *Dynamic finite-size scaling after a quench at quantum transitions*, 2018 *Phys. Rev. E* **97** 052148
- [35] Sachdev S, *Quantum Phase Transitions*, 1999 (Cambridge University Press, Cambridge)
- [36] Campostrini M, Nespolo J, Pelissetto A and Vicari E, *Finite-size scaling at first-order quantum transitions*, 2014 *Phys. Rev. Lett.* **113** 070402; *Finite-size scaling at first-order quantum transitions of quantum Potts chains*, 2015 *Phys. Rev. E* **91** 052103
- [37] Pelissetto A, Rossini D and Vicari E, *Scaling properties of the dynamics at first-order quantum transitions when boundary conditions favor one of the two phases*, 2020 *Phys. Rev. E* **102** 012143
- [38] Hänggi P, Lutz E and Talkner P, *Fluctuation theorems: Work is not an observable*, 2007 *Phys. Rev. E* **75** 050102
- [39] Campisi M, Hänggi P and Talkner P, *Colloquium: Quantum fluctuation relations: Foundations and applications*, 2011 *Rev. Mod. Phys.* **83** 771
- [40] Franchi A, Rossini D and Vicari E, *Critical crossover phenomena driven by symmetry-breaking defects at quantum transitions*, 2022 *Phys. Rev. E* **105** 034139
- [41] Campostrini M, Pelissetto A and Vicari E, *Finite-size scaling at quantum transitions*, 2014 *Phys. Rev. B* **89** 094516
- [42] Islam R, Ma R, Preiss P M, Tai M E, Lukin A, Rispoli M and Greiner M, *Measuring entanglement entropy in a quantum many-body system*, 2015 *Nature* **528** 77
- [43] Brydges T, Elben A, Jurcevic P, Vermersch B, Maier C, Lanyon B P, Zoller P, Blatt R and Roos C F, *Probing Rényi entanglement entropy via randomized measurements*, 2019 *Science* **364** 260

- [44] Debnath S, Linke N M, Figgatt C, Landsman K A, Wright K and Monroe C, *Demonstration of a small programmable quantum computer with atomic qubits*, 2016 *Nature* **536** 63
- [45] Labuhn H, Barredo D, Ravets S, de Léséleuc S, Macrì T, Lahaye T and Browaeys A, *Tunable two-dimensional arrays of single Rydberg atoms for realizing quantum Ising models*, 2016 *Nature* **534** 667
- [46] Salathè Y *et al*, *Digital quantum simulation of spin models with circuit quantum electrodynamics*, 2015 *Phys. Rev. X* **5** 021027
- [47] Cervera-Lierta A, *Exact Ising model simulation on a quantum computer*, 2018 *Quantum* **2** 114